



Published in final edited form as:

Magn Reson Med. 2018 May ; 79(5): 2555–2563. doi:10.1002/mrm.26908.

Short T_2 Imaging Using a Three-Dimensional Double Adiabatic Inversion Recovery Prepared Ultrashort Echo Time Cones (3D DIR-UTE-Cones) Sequence

Ya-Jun Ma¹, Yanchun Zhu¹, Xing Lu¹, Michael Carl², Eric Y Chang^{3,1}, and Jiang Du¹

¹Department of Radiology, University of California, San Diego, CA

²GE Healthcare, San Diego, CA

³Radiology Service, VA San Diego Healthcare System, San Diego, CA

Abstract

Purpose—To investigate high contrast imaging of short T_2 tissues with a three-dimensional double adiabatic inversion recovery prepared ultrashort echo time Cones (3D DIR-UTE-Cones) sequence.

Methods—The sequence employed two sequential adiabatic inversion pulses to suppress signals from long T_2 tissues, followed by multispoke UTE acquisition to detect signals from short T_2 tissues. The two adiabatic inversion pulses are identical with a center frequency located at the water peak but the spectral width is broad enough to cover both water and fat frequencies. The feasibility of this technique was demonstrated through numerical simulation and phantom studies. Finally, DIR-UTE-Cones was applied to three healthy volunteers to image cortical bone, patellar tendon and Achilles tendon. T_2^* was also measured via single-component exponential fitting.

Results—Numerical simulation suggests that the DIR technique provides perfect nulling of muscle and fat as well as efficient suppression of other long T_2 tissues with T_1 values between fat and water or those above water. Excellent image contrast can be achieved with DIR-UTE-Cones for the short T_2 tissues, with fitted T_2^* values of 0.28-0.38 ms for cortical bone, 0.56 ± 0.07 ms for the patella tendon, and 0.45 ± 0.06 ms for the Achilles tendon, respectively.

Conclusion—The 3D DIR-UTE-Cones sequence provides robust suppression of long T_2 tissues and allows selective imaging as well as T_2^* measurement of short T_2 tissues such as cortical bone, patellar tendon and the Achilles tendon.

Keywords

ultrashort echo time; Cones; DIR; cortical bone; tendon

Introduction

Short T_2 tissues or tissue components such as bone, calcified cartilage, ligaments, tendons, and myelin, are “invisible” with conventional clinical magnetic resonance imaging (MRI) pulse sequences because of the fast signal decay after excitation (1). Direct imaging of the short T_2 tissues or tissue components have broad applications in musculoskeletal diseases such as osteoarthritis and osteoporosis, and neurological diseases such as multiple sclerosis. A variety of ultrashort echo time (UTE) sequences and their variants have been developed for this purpose (1-4). Creating high contrast for direct imaging of short T_2 tissues or tissue components is a major challenge in UTE imaging as long T_2 tissues may have much higher signal, thus compromising short T_2 contrast (5). Suppression of signals from long T_2 tissues is a critical step in enhancing short T_2 contrast. Many techniques have been proposed for long T_2 tissue suppression which can be categorized into two types: post processing with image subtraction or summation (6-8), and selective imaging of short T_2 tissues with long T_2 saturation or inversion preparation (9-13).

The first type of approaches are always subject to signal-to-noise ratio (SNR) reduction due to image subtraction or summation as well as reduced image quality caused by the sensitiveness to susceptibility, B_0 inhomogeneity and eddy currents. Besides, most subtraction or summation based methods require two separate UTE acquisitions, leading to increased scan time and potential motion artifacts. In contrast, only a single acquisition is needed for the second type of long T_2 suppression methods. Several groups have developed techniques using long saturation pulses, followed by spoilers to selectively suppress signals from long T_2 tissues (9-13). However, these techniques are sensitive to B_1 and B_0 inhomogeneity, which may result in significant residual long T_2 signal and therefore reduced short T_2 contrast (5). The single inversion and nulling approach employs a long adiabatic inversion pulse to selectively invert and null long T_2 water and fat magnetizations, with signals from short T_2 tissues being selectively detected by subsequent UTE data acquisitions (14-20). This approach is relatively insensitive to B_1 inhomogeneity because the adiabatic inversion pulse provides uniform inversion and nulling of long T_2 magnetizations, on the condition that B_1 is above the adiabatic threshold (21). However, long T_2 water and fat typically have quite different T_1 values and this precludes simultaneous nulling of both tissues with a single inversion pulse. To accommodate this, Du et al. proposed a dual inversion recovery UTE sequence in which two long adiabatic inversion pulses centered on the water and fat resonance frequencies, respectively, are applied to account for the T_1 differences between water and fat (22). High contrast imaging of calcified cartilage can be achieved with simultaneous suppression of signals from the superficial layers of articular cartilage and marrow fat. However, this approach is sensitive to B_0 inhomogeneity due to the narrow bandwidth of the spectrally selective inversion pulse.

To overcome these challenges, we propose a new double inversion recovery prepared three-dimensional UTE Cones (3D DIR-UTE-Cones) sequence for selective short T_2 imaging. Two identical adiabatic inversion pulses with the same center frequency located at the water peak but the spectral width is broad enough are used to invert the longitudinal magnetizations of long T_2 tissues. With specific inversion times, tissues with a broad range of T_1 s, such as fat and muscle, can be well suppressed or nulled simultaneously. It is also

insensitive to B_1 inhomogeneity because of the adiabatic properties, and B_0 inhomogeneity because of the relatively wide inversion pulse bandwidth. Furthermore, multispoke acquisition per DIR preparation can be incorporated, allowing for time-efficient volumetric imaging and T_2^* quantification of short T_2 tissues ex vivo and in vivo on a clinical 3T scanner.

Theory

Features of the 3D DIR-UTE-Cones pulse sequence used in this study are shown in Figure 1. The two adiabatic inversion pulses (duration of ~ 6 ms) with specific inversion recovery times of TI_1 and TI_2 are repeated every TR period (see Fig. 1A). Following the two adiabatic inversion pulses are N_{sp} separate k-space spokes or acquisitions with an equal time interval τ for fast data acquisition. TI_1 is defined as the time between the centers of the two adiabatic inversion pulses. TI_2 is defined as the time from the center of the second adiabatic inversion pulse to the center spoke of the multispoke acquisition. A short rectangular pulse (duration of 26 to 52 μs) is used for non-selective signal excitation in each spoke (Fig. 1B), followed by 3D spiral trajectories with conical view ordering (Fig. 1C).

Adiabatic inversion pulses can effectively invert the longitudinal magnetizations of long T_2 tissues such as muscle and fat. They are also relatively immune to spatial B_1 inhomogeneity because of the adiabatic properties (21). However, the longitudinal magnetizations of short T_2 tissues (T_2^* in the range of 0.1 to 2 ms) are typically not inverted but saturated by the relatively long adiabatic inversion pulses. Here we introduce inversion efficiency factors Q_1 and Q_2 for the two adiabatic inversion pulses with a range of -1 signifying full inversion to 1 signifying no disturbance to the z-magnetization (17). Q_1 and Q_2 are equal to 0 in the condition of complete saturation.

To simplify the signal equations, T_2^* decay during the UTE excitation pulses is not taken into account (which is reasonable as the excitation pulse is much shorter than the T_2^* s of the tissues to be imaged). Within steady state, the longitudinal magnetization of the i^{th} spoke is expressed as

$$M_z^i = A(i)M_p + B(i), \quad [1]$$

where

$$A(i) = E_2 [e_1 \cos(\alpha)]^{i-1}, \quad [2]$$

$$B(i) = M_0(1 - E_2) [e_1 \cos(\alpha)]^{i-1} + M_0(1 - e_1) \{1 - [e_1 \cos(\alpha)]^{i-1}\} / [1 - e_1 \cos(\alpha)], \quad [3]$$

$$M_p = \frac{Q_1 Q_2 E_1 E_3 B_{N_{sp}} \cos(\alpha) + M_0 Q_1 Q_2 E_1 (1 - E_3) + M_0 Q_2 (1 - E_1)}{1 - Q_1 Q_2 E_1 E_3 A_{N_{sp}} \cos(\alpha)}, \quad [4]$$

using the following definitions: $A_{N_{sp}} = A(N_{sp})$, $B_{N_{sp}} = B(N_{sp})$, $E_1 = \exp(-TI_1/T_1)$, $E_2 = \exp\{-[TI_2 - \tau(N_{sp} - 1)/2]/T_1\}$, $E_3 = \exp\{-[TR - TI_1 - TI_2 - \tau(N_{sp} - 1)/2]/T_1\}$ and $e_1 = \exp(-\tau/T_1)$. M_0 is the signal intensity in the equilibrium state and α is the excitation flip angle. The explicit derivation of M_p can be found in the Appendix section.

For the short T_2 tissues, both Q_1 and Q_2 are equal to 0. Then M_p becomes 0. Therefore Eq. [1] can be simplified to $M_z^i = B(i)$. Thus, the signal of the i^{th} acquisition from the short T_2 component can be expressed as follows:

$$M_{z,s}^i = M_0(1 - E_2)[e_1 \cos(\alpha)]^{i-1} + M_0(1 - e_1)\{1 - [e_1 \cos(\alpha)]^{i-1}\}/[1 - e_1 \cos(\alpha)]. \quad [5]$$

Long T_2 Signal Suppression

When given specific TI_1 and TI_2 for the DIR preparation, it is possible to fully suppress signals from two tissues (such as muscle and fat) with different T_1 s at the same nulling point. To accelerate data acquisition, a multispoke acquisition is typically employed. When several spokes near the nulling point are acquired, long T_2 signal suppression can still be achieved since excited transverse magnetizations before the nulling point are of opposite polarity to these acquired after the nulling point. Then these transverse magnetizations will cancel in the regridding process during image reconstruction.

The magnetizations of short T_2 tissues (such as cortical bone) are not inverted, but are saturated by the two adiabatic inversion pulses. They recover to a positive longitudinal magnetization after each TI. However, the short T_2 signal intensity is mainly determined by the second TI because the second adiabatic inversion pulse always saturates the short T_2 signal regardless of how much has recovered during the first TI. As a result, a longer TI_2 will generate higher short T_2 signal.

An example illustrating how the magnetizations of fat, muscle and cortical bone change during the DIR prepared UTE sequence is shown in Fig. 2A. Since fat has a much shorter T_1 of around 340 ms compared with muscle which has a T_1 of around 1400 ms at 3T (23), the fat magnetization recovers much faster than that of muscle after the first IR pulse. The magnetization of fat demonstrates a higher degree of inversion compared with muscle immediately after the second IR pulse. As a result, it is possible that both fat and muscle magnetizations go through the nulling point simultaneously with an appropriate choice of TI_2 . The near saturated cortical bone magnetization starts to recover after the second IR pulse and it recovers very fast due to a short T_1 (24). High signal and contrast images of cortical bone will be generated when data acquisition starts near the nulling point.

The final signal intensity is proportional to the magnetization averaging of the multispoke acquisitions:

$$M_z^{\text{DIR}} = \sum_{i=1}^{N_{\text{sp}}} M_z^i / N_{\text{sp}}. \quad [6]$$

A general framework to minimize signals from long T_2 tissues for the DIR prepared sequence is expressed as follows:

$$[TI_1, TI_2] = \arg \min \left\{ \sum_{j=1}^{N_{T_1}} [m_z^{\text{DIR}}(TI_1, TI_2, TR, \alpha, \tau, N_{\text{sp}}, T_{1j})] \right\}. \quad [7]$$

Where N_{T_1} is the total number of long T_2 tissues. T_{1j} ($j = 1, 2, \dots, N_{T_1}$) is the T_1 value of the j^{th} long T_2 tissue. Given TR , α , τ and N_{sp} , TI_1 and TI_2 can be determined by Eq. [7] to achieve optimized long T_2 suppression. This framework applies for suppressing either a single tissue component with an individual T_1 value, or a group of long T_2 tissues with a range of T_1 values.

Methods

The 3D DIR-UTE-Cones sequence (see Fig. 1) was implemented on a 3T whole body scanner (MR750, GE Healthcare Technologies, Milwaukee, WI). The Cones sequence used unique k-space trajectories that sampled data along evenly spaced twisting paths in the shape of multiple cones (19,25). Data sampling started from the center of k-space and twisted outwards. Data acquisition started as soon as possible after the RF excitation with a minimal nominal echo time of 32 μs . The nominal echo time is defined as the time between the end of the rectangular pulse and the k-space center. The gradient and ADC delays were measured and used for sequence timing correction. Both RF and gradient spoiling were used to crush the remaining transverse magnetizations after each data acquisition. The 3D DIR-UTE-Cones sequence allows for anisotropic resolution (e.g., high in-plane resolution and thicker slices) for much improved SNR and reduced scan time relative to isotropic imaging. Two adiabatic inversion pulses with the same duration of 6.048 ms, bandwidth of 1.643 kHz and maximum B1 amplitude of 17 μT were used to invert or saturate long T_2 tissue components.

Simulation

Numerical simulation was performed to investigate the efficiency of the DIR preparation scheme in simultaneous suppression of signals from tissues with a range of T_1 s (200 to 2000 ms). The T_1 values of fat, muscle and bone are assumed to be 340, 1400 and 250 ms, respectively, and the proton density of bone is assumed to be 10 times less than fat and muscle. TR , α , τ and N_{sp} were 200 ms, 20°, 5 ms and 5, respectively. Optimal TI_1 and TI_2 were determined by Eq. [7]. The signal suppression efficiency of the DIR preparation scheme against T_1 was investigated.

Phantom Study

A phantom was made by combining bovine cortical bone, vegetable oil and distilled water to simulate human tissue. An 8-channel transmit/receive knee coil was used for both RF transmission and signal reception. The phantom was scanned with multiple sequences, including clinical 3D gradient recalled echo (GRE), 3D UTE-Cones and 3D DIR-UTE-Cones. The sequence parameters are listed as follows: 1) 3D GRE: TR = 15 ms, TE = 2.3 ms, flip angle = 8° , FOV = $12 \times 12 \times 8 \text{ cm}^3$, acquisition matrix = $256 \times 256 \times 20$, and scan time of 1 min 9 sec; 2) 3D UTE-Cones: TR = 20 ms, TE = 32 μs , flip angle = 15° , FOV = $12 \times 12 \times 8 \text{ cm}^3$, acquisition matrix = $256 \times 256 \times 20$, and scan time of 1 min 21 sec; 3) 3D DIR-UTE-Cones: TR = 200 ms, $\text{TI}_1/\text{TI}_2 = 100/45 \text{ ms}$ and flip angle = 20° , $N_{sp} = 5$, FOV = $16 \times 16 \times 21 \text{ cm}^3$, acquisition matrix = $128 \times 128 \times 30$, and four separate scans with TE = 32, 200, 400 and 800 μs , each with scan time of 4 min 17 sec. To null signals of both oil ($T_1 \sim 340 \text{ ms}$) and saline ($T_1 \sim 3 \text{ s}$) simultaneously, TI_1 and TI_2 of the 3D DIR-UTE-Cones sequence were calculated to be 99.7 and 45.1 ms, respectively, according to Eq. [7].

In Vivo Study

In vivo imaging was performed on three healthy male volunteers with ages of 29, 31 and 44 years. Informed consent was obtained from both subjects in accordance with guidelines of the institutional review board. An 8-channel transmit/receive knee coil was used for imaging of both tibial midshafts and knee joints, and a 10-channel receive-only flexible coil was used for imaging of the Achilles tendons. The sequence parameters used for imaging of the tibial midshafts are listed as follows: 1) 3D GRE: TR = 5.2 ms, TE = 2.4 ms, flip angle = 20° , FOV = $14 \times 14 \times 12 \text{ cm}^3$, acquisition matrix = $256 \times 256 \times 20$, and scan time = 32 sec; 2) 3D UTE-Cones: TR = 10 ms, TE = 32 μs , flip angle = 20° , FOV = $14 \times 14 \times 12 \text{ cm}^3$, acquisition matrix = $256 \times 256 \times 20$, and scan time = 1 min 15 sec; 3) 3D DIR-UTE-Cones: TR = 200 ms, $\text{TI}_1/\text{TI}_2 = 100/45 \text{ ms}$ and flip angle = 20° , $N_{sp} = 5$, FOV = $14 \times 14 \times 12 \text{ cm}^3$, acquisition matrix = $128 \times 128 \times 20$, and four separate scans with TE = 32, 200, 400 and 800 μs , with scan time = 2 min 51 sec for each TE.

The sequence parameters used for imaging of the knee joints and Achilles tendons are listed as follows: 1) 3D GRE: TR = 10 ms, TE = 2.3 ms, flip angle = 12° , FOV = $16 \times 16 \times 6 \text{ cm}^3$, acquisition matrix = $256 \times 256 \times 20$, with fat saturation, scan time = 1 min 2 sec; 2) 3D UTE-Cones: TR = 37 ms, TE = 32 μs , flip angle = 8° , FOV = $16 \times 16 \times 6 \text{ cm}^3$, acquisition matrix = $256 \times 256 \times 20$, with fat saturation, scan time = 53 sec; 3) 3D DIR-UTE-Cones: TR = 300 ms, $\text{TI}_1/\text{TI}_2 = 150/64 \text{ ms}$, flip angle = 20° , $N_{sp} = 5$, FOV = $16 \times 16 \times 6 \text{ cm}^3$, acquisition matrix = $128 \times 128 \times 20$, and four separate scans with TE = 32, 200, 400 and 800 μs , with scan time = 4 min 3 sec for each TE.

Data Analysis

The Levenberg-Marquardt algorithm was used to solve the non-linear minimization of Eq. [7]. A single exponential function was employed for T_2^* fitting of the multiple-TE DIR-UTE-Cones data. All analysis algorithms were written in Matlab (The MathWorks Inc., Natick, MA, USA) and were executed offline on the DICOM images obtained by the 3D DIR-UTE-Cones acquisition protocols described above. For each fitting both T_2^* value and the fitting error were displayed. Mean and standard deviation of T_2^* values for various short

T₂ tissues including cortical bone in the tibial midshaft, the knee joint and the ankle joint, the patellar tendon and the Achilles tendon were also reported.

Results

A numerical simulation example of fat-muscle suppression is shown in Fig. 2B. T₁ and T₂ were 99.7 and 45.1 ms, respectively, for optimal fat and muscle suppression with a TR of 200 ms. As can be seen from Fig. 2B, both fat and muscle signals are nulled. Tissues with T₁s below or above T₁ of bone are also well suppressed, suggesting that the DIR preparation scheme can provide efficient long T₂ suppression with reduced T₁ dependency. The bone signal curve is also plotted together with fat and muscle for comparison. It is necessary to mention that the x-axis is only applied to fat and muscle, but not to bone whose signal is purely determined by T₂.

Figure 3 shows images from the 3D DIR-UTE-Cones sequence on the bone phantom. With the conventional clinical 3D GRE sequence, bovine cortical bone shows as pure signal void with high signal from oil and water. The regular 3D UTE-Cones sequence shows some signal from cortical bone but poor contrast due to high signal from oil and water. With the new 3D DIR-UTE-Cones sequence, signal from oil and water are almost completely nulled, creating very high contrast for cortical bone. Fitting of the 3D DIR-UTE-Cones images with different TEs ranging from 0.032 to 0.8 ms demonstrated a short T₂* of 0.35 ± 0.01 ms for bovine cortical bone. The small standard error suggests excellent single-component decay behavior.

Figure 4 shows in vivo imaging of the leg of a 29-year-old male volunteer. Similar to the phantom study, cortical bone shows as pure signal void with the clinical 3D GRE sequence. The regular 3D UTE-Cones sequence shows signal from the cortical bone but limited contrast since the surrounding muscle and fat have much higher signal intensities. In contrast, the 3D DIR-UTE-Cones sequence shows high signal from the cortex of the tibial midshaft, with near zero signal from both muscle and marrow fat. Tendons and aponeuroses as well as coil elements also show as high signal. These results confirm that the DIR technique allows nulling of both muscle and marrow fat, despite the large differences in T₁ relaxation times. Exponential fitting of the 3D DIR-UTE-Cones images with different TEs demonstrates a short T₂* of 0.36 ± 0.02 ms for the tibial midshaft cortex in this volunteer.

Figure 5 shows in vivo images of the knee joint in a 31-year-old male volunteer. The clinical fat suppressed 3D GRE sequence provides high signal and contrast imaging of long T₂ tissues such as the femoral and tibial articular cartilage and muscle, with little or no signal from patellar tendon and cortical bone. The regular fat-saturated 3D UTE-Cones sequence shows similar results with little image contrast for patellar tendon and cortical bone, largely due to the high signal from long T₂ tissues such as articular cartilage and muscle, although fat signal was suppressed using a chemical shift-based fat saturation pulse. Again, images from the 3D DIR-UTE-Cones sequence show high contrast for short T₂ tissues such as patellar tendon and cortical bone, with excellent suppression of both long T₂ water signals (such as muscle and articular cartilage) and marrow fat. Exponential fitting of the 3D DIR-UTE-Cones images with different TEs demonstrates a short T₂* of 0.3 ± 0.03 ms for the thin

layer of cortical bone and 0.38 ± 0.02 ms for the patellar bone in the knee joint, and slightly longer T_2^* of 0.5 ± 0.07 ms for the patellar tendon.

Figure 6 shows in vivo images of the ankle joint of a 29-year-old male volunteer. The clinical fat suppressed 3D GRE sequence provides near zero signal for cortical bone and the Achilles tendon with high signal for long T_2 muscle. Both cortical bone and the Achilles tendon are still poorly visualized with the regular fat saturated 3D UTE-Cones sequence mostly due to the much higher signal from surrounding muscle. Fat signal was largely suppressed by the fat saturation pulse. Similar to results in the knee joint study, the 3D DIR-UTE-Cones sequence shows excellent image contrast for both cortical bone and the Achilles tendon. Both muscle and marrow fat are efficiently suppressed by the DIR preparation pulse. Excellent exponential fitting of the 3D DIR-UTE-Cones images with different TEs was achieved for both cortical bone and the Achilles tendon, with fitted T_2^* values of 0.29 ± 0.01 ms and 0.42 ± 0.05 ms, respectively.

Table 1 summarizes the mean and standard deviation of T_2^* values for cortical bone, patellar tendon and Achilles tendon for three healthy volunteers. As can be seen, very consistent T_2^* values were observed for those short T_2 tissues in vivo, which further confirms the robustness of the DIR technique in suppressing long T_2 signals (minimizing long T_2 signal contamination when imaging short T_2 tissues and measuring their T_2^* s).

Discussion

We have demonstrated in this study that the 3D DIR-UTE-Cones sequence can simultaneously suppress signals from long- T_2 water and fat, and provide excellent image contrast for short- T_2 tissues such as cortical bone, the patellar tendon and the Achilles tendon. Our simulation study suggests that the DIR technique provides perfect nulling of two tissues with distinct T_1 s such as muscle and marrow fat. In addition, the DIR technique provides good suppression of long T_2 tissues whose T_1 s are between fat and water T_1 s, or slightly longer than water T_1 s. Our ex vivo and in vivo studies demonstrate the robust nature of the 3D DIR-UTE-Cones sequence in suppressing long T_2 water and fat signals in the lower extremity, the knee joint and the ankle joint. Furthermore, the 3D DIR-UTE-Cones sequence allows quantitative imaging of short T_2 tissues with excellent T_2^* measurement.

The new DIR preparation scheme bears some similarity with our older version of dual inversion recovery preparation (22). Both techniques are based on the inversion and nulling concept, employing two adiabatic inversion pulses to null signals from tissues with two distinct T_1 s. In the previous dual inversion recovery preparation scheme, the two adiabatic inversion pulses were applied at two distinct resonance frequencies to cover the expected water and fat peaks, respectively. UTE acquisitions began when the inverted longitudinal magnetizations of water and fat reached the nulling point. The major challenge associated with this technique was the requirement of two adiabatic inversion pulses with relatively narrow, but separate spectral profiles. Any overlap between the two spectral profiles potentially resulted in re-inversion of the long T_2 magnetization, leading to imperfect signal nulling and thus long T_2 signal contamination. Further, this technique was sensitive to off-resonance effects. When the peak frequencies of fat and water were shifted out of the

spectral coverage, due to susceptibility such as from air-tissue interfaces or other factors, the dual inversion recovery technique would fail, leading to long T_2 signal contamination. Moreover, this technique was less efficient in the setting of multiple tissues with T_1 values away from the T_1 s of water and fat.

On the other hand, the new DIR preparation scheme employs two identical adiabatic inversion pulses with relatively broad spectral coverage of 1.643 kHz. Both pulses are centered on the water peak but broad enough to cover various fat peaks (26). As a result, the DIR scheme is insensitive to off-resonance effects, providing excellent long T_2 suppression even for tissues with boundaries near air, as demonstrated in the in vivo studies of knee and ankle joints. There is little residual signal from water and fat near the skin where long T_2 suppression is typically more challenging. The DIR preparation scheme is insensitive to B_1 inhomogeneity as long as the amplitudes of both inversion pulses are above the adiabatic threshold (21). More importantly, the new DIR technique provides efficient suppression of tissues with a broad range of T_1 s. This is a major advantage over the single adiabatic inversion recovery or dual adiabatic inversion recovery preparation techniques where signal from the skin is less suppressed likely due to different T_1 values as well as off-resonance associated with the air-tissue interface (17, 22). The olefinic protons in the fatty acid chains which are located close to the water peak are typically difficult to suppress with single or dual adiabatic inversion recovery preparation, and are expected to be better suppressed with the DIR preparation scheme (26). In addition, the single IR expression can be easily derived from the proposed DIR frame by setting Q_1 or Q_2 to 1 (19).

The bone signal reduction can be calculated by $S = M_0 E_2$ for a single spoke acquisition, which is derived from Eq. [5]. With a T_1 of 250 ms and TI_2 of 64ms, the bone signal reduction is $0.77 M_0$. Though large amounts of bone signal have not been acquired, the DIR-UTE-Cones images still show high bone contrast since soft tissues signals were almost suppressed perfectly. In addition, the DIR-UTE-Cones is less time-efficient than the conventional UTE-Cones sequence since a DIR preparation is used. With the same TR of 200 ms and excitation flip angle of 20° , the specific absorption ratios (SAR) are 1.5 W/kg and 0.1W/kg detected by SAR monitor for the DIR-UTE-Cones and conventional UTE-Cones sequences respectively. Though the SAR of DIR-UTE-Cones is much higher than conventional UTE-Cones sequence, it remains far below the SAR limit of 12 W/kg for knee imaging.

The DIR-UTE-Cones sequence can readily be used for imaging of other short- T_2 species, such as the calcified cartilage where simultaneous suppression of superficial layers of articular cartilage and marrow fat is essential for high contrast imaging of calcified cartilage (22). Other applications include direct imaging of myelin protons in white matter of the brain and spinal cord, where efficient suppression of water protons is essential for selective imaging of myelin protons (27-29). Different groups of water protons, such as those in cerebrospinal fluid, extra- and intra-cellular water and water trapped in the myelin bilayers may have different T_1 s (30). The DIR-UTE-Cones sequence may provide more efficient suppression of the various water groups regardless of their different T_1 s, therefore greatly improving the specificity in myelin imaging. Future work will be performed on optimizing the DIR-UTE-Cones sequence for volumetric myelin mapping ex vivo and in vivo.

Since the DIR-UTE-Cones sequence allows selective imaging of short T_2 tissues, it can also be used for quantitative evaluation of T_1 and T_2^* relaxation times as well as proton density. Long T_2 signal contamination is typically a major source of error in quantitative UTE imaging (5). The DIR-UTE-Cones acquisition together with a calibration phantom may also provide volumetric mapping of proton density for short T_2 tissues.

This study has several limitations. First, the efficiency of the 3D DIR-UTE-Cones sequence in terms of signal to noise ratio (SNR) and contrast to noise ratio (CNR) per unit acquisition time has not been evaluated or compared with existing techniques such as single or dual adiabatic inversion recovery preparation based techniques, on-resonance or off-resonance saturation based techniques, and subtraction or summation based techniques. We have only demonstrated the technical feasibility of the 3D DIR-UTE-Cones sequence in providing high contrast volumetric imaging of short T_2 tissues ex vivo and in vivo. Second, the 3D DIR-UTE-Cones sequence has only been investigated in imaging short T_2 tissues in the musculoskeletal systems including the knee and ankle joints. This technique may have broad applications in neurological, body or vascular diseases such as myelin centric or leukodystrophic disorders and soft tissue calcifications in the breast or carotid plaques.

Conclusion

The 3D DIR-UTE-Cones sequence provides robust suppression of long T_2 tissues with a broad range of T_1 s, and allows selective imaging of short T_2 tissues such as cortical bone, patellar tendon and the Achilles tendon ex vivo and in vivo on a clinical 3T scanner. The 3D DIR-UTE-Cones sequence also provides quantitative information such as estimation of T_2^* relaxation time without long T_2 signal contamination.

Supplementary Material

Refer to Web version on PubMed Central for supplementary material.

Acknowledgments

The authors acknowledge grant support from GE Healthcare and NIH (1R01 AR062581 and 1R01 AR068987) and the VA Clinical Science R&D Service (1101CX001388).

Appendix

The element timing of the DIR multispoke sequence is shown in Supporting Figure S1. t_1 is the duration between the second IR pulse and the first excitation pulse. t_2 is the duration between the last excitation pulse and the first IR pulse. $M_{z,1}$, $M_{z,2}$, $M_{z,3}$, $M_{z,4}$ and M_p are the longitudinal magnetizations after the last excitation pulse, before the first IR pulse, after the first IR pulse, before the second IR pulse and after the second IR pulse, respectively. According to Bloch equations, the relations of the above five magnetizations are expressed as follows:

$$M_{z,1} = (M_p A_{N_{sp}} + B_{N_{sp}}) \cos(\alpha), \quad [A1]$$

$$M_{z,2}=M_{z,1}\exp(-t_2/T_1)+M_0[1-\exp(-t_2/T_1)], \quad [\text{A2}]$$

$$M_{z,3}=Q_1M_{z,2}, \quad [\text{A3}]$$

$$M_{z,4}=M_{z,3}\exp(-t_1/T_1)+M_0[1-\exp(-t_1/T_1)], \quad [\text{A4}]$$

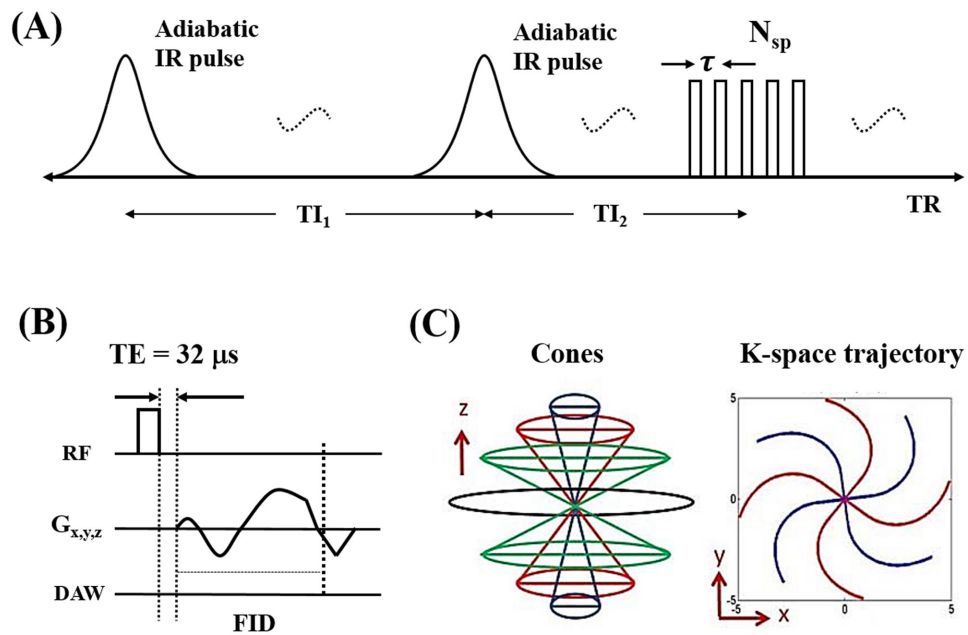
$$M_p=Q_2M_{z,4}, \quad [\text{A5}]$$

where $t_1=TR-\tau(N_{sp}-1)/2/T_1$ and $t_2=TR-TI_1-TI_2-\tau(N_{sp}-1)/2/T_1$. $A_{N_{sp}}$ and $B_{N_{sp}}$ are defined in the Theory section. Thus, M_p is determined from Eq. [A1]-[A5], whose final expression is shown in Eq. [4].

References

1. Gatehouse PD, Bydder GM. Magnetic resonance imaging of short T2 components in tissue. *Clin Radiol.* 2003; 58:1–19. [PubMed: 12565203]
2. Idiyatullin D, Corum C, Park JY, Garwood M. Fast and quiet MRI using a swept radiofrequency. *J Magn Reson.* 2006; 181:342–349. [PubMed: 16782371]
3. Grodzki DM, Jakob PM, Heismann B. Ultrashort echo time imaging using pointwise encoding time reduction with radial acquisition (PETRA). *Magn Reson Med.* 2012; 67:510–518. [PubMed: 21721039]
4. Weiger M, Pruessmann KP, Hennel F. MRI with zero echo time: hard versus sweep pulse excitation. *Magn Reson Med.* 2011; 66:379–389. [PubMed: 21381099]
5. Du J, Bydder GM. Qualitative and quantitative ultrashort-TE MRI of cortical bone. *NMR Biomed.* 2013; 26:489–506. [PubMed: 23280581]
6. Larson PE, Conolly SM, Pauly JM, Nishimura DG. Using adiabatic inversion pulses for long-T2 suppression in ultrashort echo time (UTE) imaging. *Magn Reson Med.* 2007; 58:952–961. [PubMed: 17969119]
7. Du J, Takahashi AM, Bydder M, Chung CB, Bydder GM. Ultrashort TE imaging with off-resonance saturation contrast (UTE-OSC). *Magn Reson Med.* 2009; 62:527–531. [PubMed: 19449436]
8. Johnson EM, Vyas U, Ghanouni P, Pauly KB, Pauly JM. Improved Cortical Bone Specificity in UTE MR Imaging. *Magn Reson Med.* 2017; 77:684–695. [PubMed: 26972442]
9. Rahmer J, Bornert P, Groen J, Bos C. Three-dimensional radial ultrashort echo-time imaging with T2 adapted sampling. *Magn Reson Med.* 2006; 55:1075–1082. [PubMed: 16538604]
10. Techawiboonwong A, Song HK, Wehrli FW. In vivo MRI of submillisecond T2 species with two-dimensional and three-dimensional radial sequences and applications to the measurement of cortical bone water. *NMR Biomed.* 2008; 21:59–70. [PubMed: 17506113]
11. Pauly, JM., Conolly, SM., Macovski, A. Proceedings of the 10th Annual Meeting of SMRI. New York: 1992. Suppression of long T2 components for short T2 imaging; p. 330
12. Sussman MS, Pauly JM, Wright GA. Design of practical T2-selective RF excitation (TELEX) pulses. *Magn Reson Med.* 1998; 40:890–899. [PubMed: 9840834]

13. Larson PE, Gurney PT, Nayak K, Gold GE, Pauly JM, Nishimura DG. Designing long-T2 suppression pulses for ultrashort echo time imaging. *Magn Reson Med*. 2006; 56:94–103. [PubMed: 16724304]
14. Robson MD, Gatehouse PD, Bydder M, Bydder GM. Magnetic resonance: an introduction to ultrashort TE (UTE) imaging. *J Comput Assist Tomogr*. 2003; 27:825–846. [PubMed: 14600447]
15. Reichert ILH, Robson MD, Gatehouse PD, He T, Chappell KE, Holmes J, Girgis S, Bydder GM. Magnetic resonance imaging of cortical bone with ultrashort TE (UTE) pulse sequences. *Magn Reson Imag*. 2005; 23:611–618.
16. Du J, Hamilton G, Takahashi A, Bydder M, Chung CB. Ultrashort TE spectroscopic imaging (UTESI) of cortical bone. *Magn Reson Med*. 2007; 58:1001–1009. [PubMed: 17969110]
17. Du J, Carl M, Bydder M, Takahashi A, Chung CB, Bydder GM. Qualitative and quantitative ultrashort echo time (UTE) imaging of cortical bone. *J Magn Reson*. 2010; 207:304–311. [PubMed: 20980179]
18. Du J, Bydder M, Takahashi AM, Carl M, Chung CB, Bydder GM. Short T2 contrast with three-dimensional ultrashort echo time imaging. *Magn Reson Imaging*. 2011; 29:470–482. [PubMed: 21440400]
19. Carl M, Bydder GM, Du J. UTE imaging with simultaneous water and fat signal suppression using a time-efficient multispoke inversion recovery pulse sequence. *Magn Reson Med*. 2016; 76:577–582. [PubMed: 26309221]
20. Li C, Magland JF, Zhao X, Seifert AC, Wehrli FW. Selective in vivo bone imaging with long-T2 suppressed PETRA MRI. *Magn Reson Med*. 2017; 77:989–997. [PubMed: 26914767]
21. Garwood M, DelaBarre L. The return of the frequency sweep: designingadiabatic pulses for contemporary NMR. *J Magn Reson*. 2001; 153:155–177. [PubMed: 11740891]
22. Du J, Takahashi AM, Bae WC, Chung CB, Bydder GM. Dual inversion recovery, ultrashort echo time (DIR UTE) imaging: creating high contrast for short-T2 species. *Magn Reson Med*. 2010; 63:447–455. [PubMed: 20099332]
23. Gold GE, Han E, Stainsby J, Wright G, Brittain J, Beaulieu C. Musculoskeletal MRI at 3.0T: relaxation times and image contrast. *AJR*. 2004; 183:343–351. [PubMed: 15269023]
24. Chen J, Chang EY, Carl M, Ma Y, Shao H, Chen BM, Wu Z, Du J. Measurement of bound and pore water T1 relaxation times in cortical bone using three-dimensional ultrashort echo time cones sequences. *Magn Reson Med*. 2016; doi: 10.1002/mrm.25872
25. Gurney PT, Hargreaves BA, Nishimura DG. Design and analysis of a practical 3D cones trajectory. *Magn Reson Med*. 2006; 55:575–582. [PubMed: 16450366]
26. Hamilton G, Yokoo T, Bydder M, Cruite I, Schroeder ME, Sirlin CB, Middleton MS. In vivo characterization of the liver fat 1H NMR spectrum. *NMR Biomed*. 2011; 24:784–790. [PubMed: 21834002]
27. Horch RA, Gore JC, Does MD. Origins of the ultrashort-T2 1H NMR signals in myelinated nerve: a direct measure of myelin content? *Magn Reson Med*. 2011; 66(1):24–31. [PubMed: 21574183]
28. Wilhelm MJ, Ong HH, Wehrli SL, Li C, Tsai PH, Hackney DB, Wehrli FW. Direct magnetic resonance detection of myelin and prospects for quantitative imaging of myelin density. *P Natl Acad Sci USA*. 2012; 109(24):9605–9610.
29. Sheth V, Shao H, Chen J, Vandenberg S, Corey-Bloom J, Bydder GM, Du J. Magnetic resonance imaging of myelin using ultrashort Echo time (UTE) pulse sequences: Phantom, specimen, volunteer and multiple sclerosis patient studies. *Neuroimage*. 2016; 136:37–44. [PubMed: 27155128]
30. Deoni SCL, Rutt BK, Arun T, Pierpaoli C, Jones DK. Gleaning multicomponent T1 and T2 information steady-state imaging data. *Magn Reson Med*. 2008; 60:1372–1387. [PubMed: 19025904]

**Figure 1.**

The 3D DIR-UTE-Cones sequence employs two adiabatic inversion pulses for long T₂ suppression, followed by 3D UTE-Cones data acquisition (A). In the basic 3D UTE-Cones sequence a short rectangular pulse is used for signal excitation followed by 3D spiral sampling with a minimal nominal TE of 32 μ s (B). The spiral trajectories are arranged with conical view ordering (C). To speed up data acquisition, multiple spokes can be sampled after each long T₂ preparation (A).

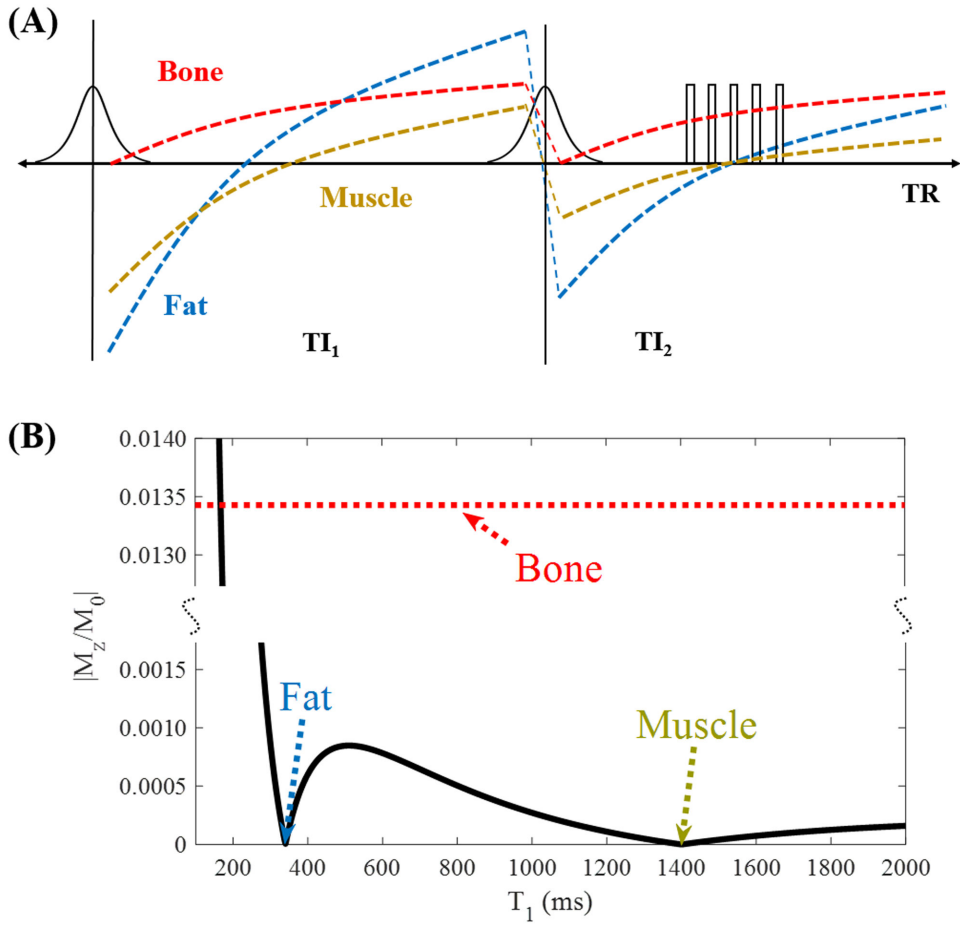


Figure 2. With DIR preparation, two adiabatic inversion pulses are applied sequentially using two different inversion times of TI_1 and TI_2 to invert and null the longitudinal magnetizations of long T_2 muscle and fat, followed by multispoke 3D UTE-Cones data acquisition (A). Numerical simulation shows high contrast imaging of cortical bone with excellent suppression of tissues with a broad range of T_1 s including muscle and fat (B).

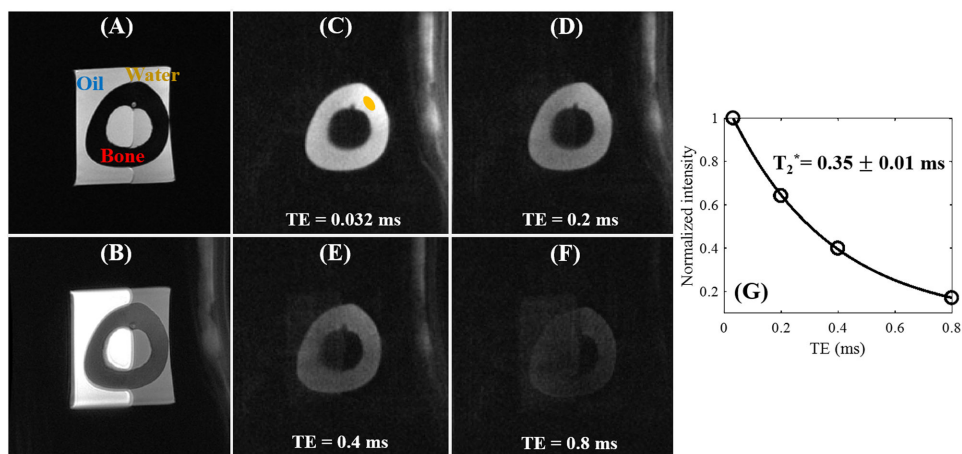


Figure 3. Evaluation of the 3D DIR-UTE-Cones sequence on a phantom consisting of a piece of bovine cortical bone soaked in pure corn oil and distilled water. The clinical 3D GRE sequence shows high signal for corn oil and water but zero signal for bone (A). The basic 3D UTE-Cones sequence shows high signal for oil and water, and low signal for bone with little contrast (B). The 3D DIR-UTE-Cones sequence shows simultaneous suppression of oil and water, providing excellent image contrast for cortical bone with TEs of 0.032 ms (C), 0.2 ms (D), 0.4 ms (E), and 0.8 ms (F). Excellent single-component fitting was achieved for bovine cortical bone demonstrating a short T_2^* of 0.35 ± 0.01 ms (G).

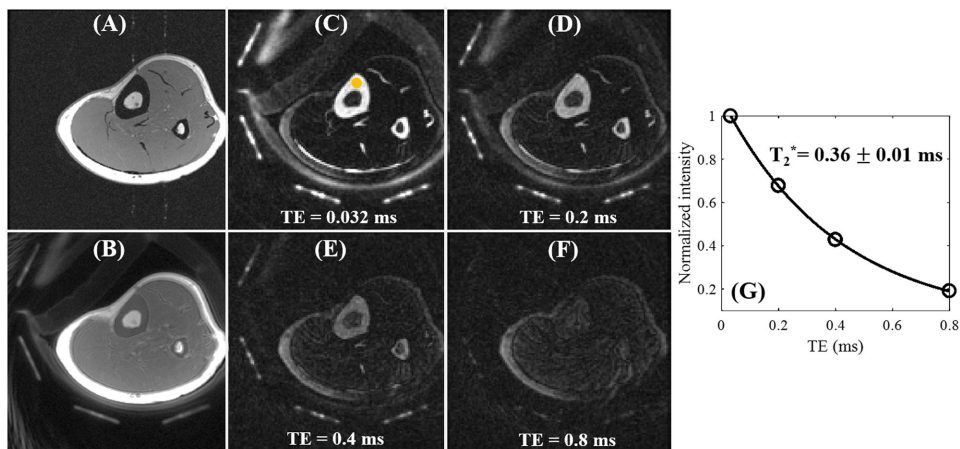


Figure 4.

In vivo imaging of the left leg of a 29-year-old male volunteer with a clinical 3D GRE sequence where cortical bone shows as a pure signal void (A). The basic 3D UTE-Cones sequence shows cortical bone signal, but with low contrast (B). The 3D DIR-UTE-Cones sequence shows simultaneous suppression of muscle and marrow fat, providing excellent image contrast for cortical bone, tendons and aponeurosis with TEs of 0.032 ms (C), 0.2 ms (D), 0.4 ms (E), and 0.8 ms (F). Excellent single-component fitting was achieved for tibial midshaft cortex with a short T_2^* of 0.36 ± 0.01 ms (G).

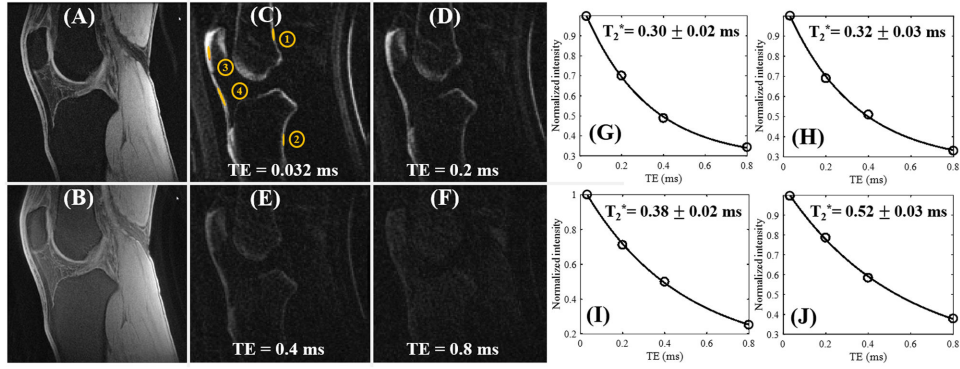


Figure 5.

In vivo imaging of the knee joint of a 31-year-old male volunteer with a clinical 3D GRE sequence where cortical bone and patellar tendon show as pure signal void (A). The basic 3D UTE-Cones sequence shows little contrast for cortical bone and patellar tendon (B). The 3D DIR-UTE-Cones sequence shows simultaneous suppression of muscle and marrow fat, providing excellent image contrast for cortical bone (ROIs #1 and #2), patellar bone (ROI #3) and patellar tendon (ROI #4) with TEs of 0.032 ms (C), 0.2 ms (D), 0.4 ms (E), and 0.8 ms (F). Excellent single-component fitting was achieved for cortical bone demonstrating a short T_2^* of 0.30 ± 0.02 ms for ROI #1 (G) and 0.32 ± 0.03 ms for ROI #2 (H), and for patellar bone demonstrating a short T_2^* of 0.38 ± 0.02 ms for ROI #3 (I) and for patellar tendon demonstrating a short T_2^* of 0.52 ± 0.03 ms for ROI #4 (J).

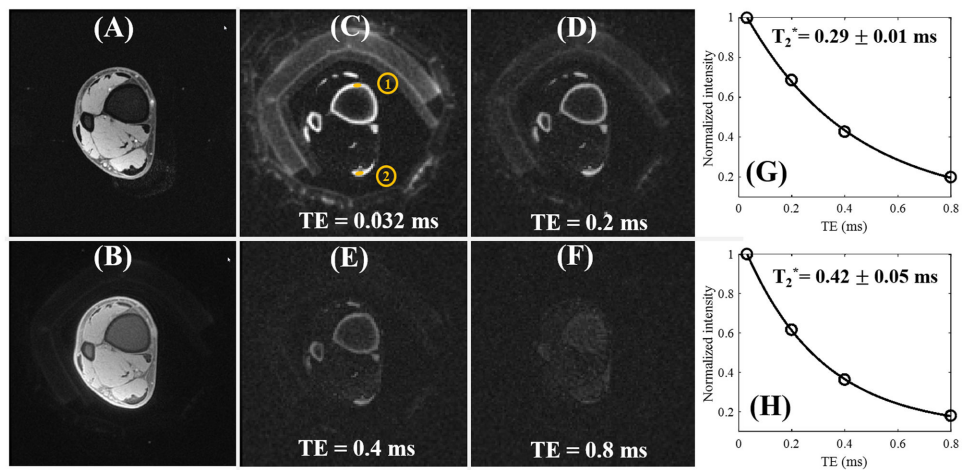


Figure 6.

In vivo imaging of the ankle joint of a 29-year-old male volunteer with a clinical 3D GRE sequence where cortical bone and the Achilles tendon show as pure signal void (A). The basic 3D UTE-Cones sequence shows little contrast for cortical bone and the Achilles tendon (B). The 3D DIR-UTE-Cones sequence shows simultaneous suppression of muscle and marrow fat, providing excellent image contrast for cortical bone (ROI #1) and the Achilles tendon (ROI #2) with TEs of 0.032 ms (C), 0.2 ms (D), 0.4 ms (E), and 0.8 ms (F). Excellent single-component fitting was achieved for cortical bone in the ankle demonstrating a short T_2^* of 0.29 ± 0.01 ms (G), and for the Achilles tendon demonstrating a short T_2^* of 0.42 ± 0.05 ms (H).

Mean and standard deviations of T_2^* values (ms) of in vivo bone and tendon data (3 healthy volunteers) acquired by 3D DIR-UTE-Cones sequence.

Table 1

T_2^* (ms)	Cortical bone (tibia)	Cortical bone (femur)	Patella bone	Patella tendon	Achilles tendon
Tibia	0.37±0.02				
Knee	0.34±0.02	0.32±0.03	0.38±0.02	0.56±0.07	
Ankle	0.28±0.04				0.45±0.06